Comparison of Josephson fluxon modes in high- and low-temperature superconducting stacked Josephson junctions

V. M. Krasnov,* V. A. Oboznov, and V. V. Ryazanov
Institute of Solid State Physics, 142432 Chernogolovka, Russia

N. Mros, A. Yurgens,† and D. Winkler‡
Department of Microelectronics and Nanoscience, Chalmers University of Technology, S-41296 Göteborg, Sweden
(Received 25 June 1999)

We experimentally study and compare the perpendicular (*c*-axis) transport properties of layered high-T_c superconductor (HTSC) $Bi_2Sr_2CaCu_2O_{8+x}$ and low-T_c (LTSC) Nb/Cu multilayers. Both for HTSC and LTSC samples similar anomalous features were observed. (i) The *c*-axis critical current I_c is multiple valued as a function of temperature T and in-plane magnetic field H. (ii) I_c exhibits extremely large fluctuations and the probability distribution $P(I_c)$ has multiple maxima. (iii) The $I_c(H)$ patterns are aperiodic. (iv) In the dynamic state, the flux-flow branches in current-voltage characteristics consist of multiple closely spaced sub-branches and exhibit large fluctuations due to switching between the sub-branches. Experimental data are in qualitative agreement with numerical simulations for the stack of long strongly coupled Josephson junctions. All this is taken as an evidence for the existence of multiple quasiequilibrium Josephson fluxon modes in our samples. From the study of LTSC multilayers we have found one-to-one correspondence between the anomalous behavior and appearance of stacked Josephson junctions in the two-dimensional state.

I. INTRODUCTION

Vortex related properties of layered superconductors have been extensively studied in the last decade especially in connection with high-T_c superconductors (HTSC). Highly anisotropic HTSC compounds exhibit well defined two-dimensional (2D) properties and can be considered as stacks of 2D atomic scale superconducting layers (*ab* planes) with Josephson coupling between them. Such intrinsic stacked Josephson junctions (SJJ's) could be promising objects for applications in cryoelectronics.

Physical properties of intrinsic SJJ's are qualitatively different from that of anisotropic three-dimensional (3D) superconductors. This is reflected in the vortex structure for magnetic field parallel and perpendicular to the superconducting (*S*) layers. In a perpendicular field (along the *c* axis) the vortex consists of a number of 2D pancake vortices in each *S* layer.[1] The pancake vortices are of Abricosov type and have a normal core and circulating supercurrents in the *ab* plane with a characteristic length λ_{ab}. Properties of such vortices are well studied, for a review see, e.g., Ref. 2, and we will not consider those here. A transition from three-to-two-dimensional vortex system via a smectic phase, commensurate with the layered structure of superconductor, was studied in Ref. 3 for parallel and slightly tilted magnetic fields with respect to the *ab* plane. The commensurability is due to intrinsic pinning,[4] which tends to locate parallel vortices between *S* layers. Such vortices (fluxons) are of Josephson type. They have circulating currents flowing both along and across *S* layers and do not have the normal core.

The shape of a single fluxon in layered superconductors at large distances from the fluxon center was studied in Refs. 5, 6 for identical and nonidentical layers, respectively. It was shown, that the magnetic field of the fluxon is extended over many layers with the characteristic length $\sim\lambda_{ab}$ along the *c* axis. For the case of SJJ's with a limited number of junctions, the shape of the single fluxon has been studied in Refs. 7–9. It was shown that fluxon shape could be considerably different from that in a single Josephson junction, especially in the dynamic case.[9] At large parallel magnetic field, Josephson vortices are believed to form a regular fluxon lattice (FL) due to repulsive fluxon interaction. Since fluxons are spread over a large number of layers, it may not be favorable to have a perfect translational symmetry along the *c* axis, needed for a triangular FL, and the FL may be rhombic.[10] However, the perfect FL can be achieved only at large magnetic fields, when the spacing between fluxons along the *ab* plane is of the order of the Josephson penetration depth $\lambda_J = \gamma s$, where γ is the anisotropy factor and s is the stacking periodicity. The corresponding field $\Phi_0/\gamma s^2$, is of the order of 1T for Bi and Tl based HTSC's. This field is much larger than the lower critical field[11,12] $H_{c1}^{\parallel}\sim$mT.

The fluxon distribution in layered superconductors at low fields $H_{c1}^{\parallel}<H<\Phi_0/\gamma s^2$, is still a matter of controversy. Levitov[10] have found ''phyllotaxis'' and bifurcations in the FL at low fields, due to existence of multiple metastable FL's with approximately equal energies. In Ref. 13, this approach was extended using a ''growth'' algorithm, allowing variation in the FL along the *c* axis. Although restricted to constant space periodicity both along and across layers, the model showed the existence of a large variety of quasi periodic or aperiodic fluxon configurations in the *c*-axis direction. At low fields, the fluxon system becomes completely frustrated and tends to be chaotic.[13] Recent numerical simulations revealed that fluxons in SJJ's may from buckled chains[14,15] instead of the regular FL. Clearly, the lattice description of fluxon distribution in SJJ's becomes unappropriate at low magnetic fields.

Recently, a fluxon mode approach was developed for the

analysis of fluxon distribution in SJJ's with a small number of junctions and fluxons.[8] It was shown that for given external conditions, multiple quasiequilibrium fluxon configurations (modes) exist in long, $L \gg \lambda_J$, strongly coupled SJJ's. The modes are characterized by different fluxon distributions in the stack and do not have a priori any translational symmetry. We will use a string $(n_1,\ldots,n_i,\ldots,n_N)$ as a short notation of fluxon modes, where n_i is a number of fluxons in junction i and N is the number of junctions in the stack. For example the mode (1, 0, 0) corresponds to a single fluxon in junction 1 in a stack of three Josephson junctions. Due to existence of multiple quasiequilibrium fluxon modes, the state of the stack for given external conditions (magnetic field H and temperature T) is not well defined. It can be described only statistically with a certain probability of being in any of the modes. Neither the number of fluxons in each junction nor even the total number of fluxons in the stack is fixed for given H and T. In Ref. 16, the existence of fluxon submodes was shown, which have the same number of fluxons but are different with respect to fluxon sequence and symmetry of the phase difference in the junctions (along the *ab* plane). In experiment, multiple fluxon modes and submodes result in multiple valued *c*-axis critical current I_c,[17] and a complicated aperiodic $I_c(H)$ dependence.[16] Moreover, since different fluxon modes/submodes may have similar energies, the fluxon system is frustrated and may exhibit strong fluctuations. This may account for unusual *c*-axis transport properties of $Bi_2Sr_2CaCu_2O_{8+x}$ (Bi2212) mesas.[17,16] Due to difficulties in interpretation of HTSC data, the study of model artificial low-T_c (LTSC) layered structures with well defined and controllable parameters is of particular interest.

In this paper we present a comprehensive study of multiple Josephson fluxon modes in HTSC Bi2212 mesas and LTSC Nb/Cu multilayers (ML's). Similar anomalous behavior was observed both for LTSC and HTSC structures. Namely, it was shown that the *c*-axis critical current is multiple valued as a function of temperature and parallel magnetic field and exhibits strong fluctuations. In the dynamic state, the flux-flow branch appears in the current-voltage characteristics (IVC's). It consists of multiple closely spaced subbranches. Experimental data are in agreement with numerical simulations and implies the existence of multiple quasiequilibrium fluxon modes and submodes in long strongly coupled SJJ's. Moreover, from the study of LTSC ML's we unambiguously correlate the appearance of anomalous behavior with the appearance of SJJ's in the ML, when it undergoes the 3D-2D crossover.

The paper is organized in the following way. In Section II we introduce the coupled sine-Gordon equation,[7] which is used for numerical simulations. In Sec. III the samples are described. In Sec. IV we present main experimental and numerical results relevant to observation of fluxon modes in layered superconductors. The section is subdivided into four subsections: (A) temperature dependence of the critical current; (B) magnetic field dependence of the critical current; (C) the lower critical field and ineffectiveness of screening; and (D) observation of multiple flux-flow subbranches. Throughout the section we compare HTSC and LTSC data with numerical simulations. Finally, we discuss the obtained results and make the conclusions.

II. GENERAL RELATIONS

First, we briefly describe the formalism of the coupled sine-Gordon equation used in our numerical simulations. More details can be found in Ref. 8. We consider a stack with the overlap geometry, consisting of N junctions with the following parameters: J_{ci} the critical current density C_i and R_i, the capacitance and the quasiparticle resistance per unit area, respectively, t_i, the thickness of the tunnel barrier between the layers, d_i and λ_{Si}, the thickness and London penetration depth of S layers, and L, L_y, the lengths of the stack along the x and y axes, respectively. The elements of the stack are numerated from the bottom to the top, so that junction i consists of superconducting layers i, $i+1$ and the tunnel barrier i.

The gauge invariant phase difference, φ_i, in long SJJ's can be described by the coupled sine-Gordon equation[7]

$$\varphi'' = \mathbf{A}\cdot\mathbf{J}_z - \mathbf{J}_b . \tag{1}$$

Here φ is the column of φ_i, ''primes'' denote spatial derivatives along the junction length, $\mathbf{A}$ is a symmetric tridiagonal $N\times N$ matrix the only nonzero elements of which are

$$A_{i,i-1} = -S_i/\Lambda_1;\ \ A_{i,i} = \Lambda_i/\Lambda_1;\ \ A_{i,i+1} = -S_{i+1}/\Lambda_1 .$$

Here

$$\Lambda_i = t_i + \lambda_{Si}\coth\left(\frac{d_i}{\lambda_{Si}}\right) + \lambda_{Si+1}\coth\left(\frac{d_{i+1}}{\lambda_{Si+1}}\right),$$

$$S_i = \lambda_{Si}\,\mathrm{cosech}\left(\frac{d_i}{\lambda_{Si}}\right).$$

$\mathbf{J}_z$ is the vector representing the current density across the junctions, which consists of three main components: the supercurrent, the displacement current and the normal (quasiparticle) current:

$$J_{zi} = \frac{J_{ci}}{J_{c1}}\sin(\varphi_i) + \frac{C_i}{C_1}\,\ddot{\varphi}_i + \alpha_1\frac{R_1}{R_i}\,\dot{\varphi}_i . \tag{2}$$

Here dots denote time derivatives and $\alpha_1 = \sqrt{\Phi_0/2\pi c J_{c1} C_1 R_1^2}$ is the damping parameter of junction 1, Φ_0 is the flux quantum and c is the velocity of light in vacuum.

In Eq. (1), $\mathbf{J}_b$ represents the bias current density and for arbitrary bias configuration can be written as[8]

$$J_{bi} = \frac{\Lambda_i^*}{2J_{c1}\Lambda_1}\left[\sum_{i+2}^{N+1}\Delta J_{yj} - \sum_{1}^{i-1}\Delta J_{yj} + \left(1+\frac{2S_{i+1}}{\Lambda_i^*}\right)\Delta J_{yi+1} - \left(1+\frac{2S_i}{\Lambda_i^*}\right)\Delta J_{yi}\right], \tag{3}$$

where $\Delta J_{yi} = [I_{yi}(L_y) - I_{yi}(0)]/(LL_y)$, and

$$\Lambda_i^* = \Lambda_i - S_i - S_{i+1} \tag{4}$$

is the effective magnetic thickness of junction i. In Eq. (1) we have normalized space and time to the Josephson penetration depth, $\lambda_{j1} = \sqrt{\Phi_0 c/8\pi^2 J_{c1}\Lambda_1}$, and the inverse

plasma frequency of a single junction 1, $1/\omega_{p1} = \sqrt{\Phi_0 C_1/2\pi c J_{c1}}$, respectively.

Equation (1) should be supplemented by the boundary conditions

$$\varphi_1' = 2\frac{H\Lambda_i^*}{H_0\Lambda_1}, \quad (x=0,L). \tag{5}$$

Here H is the applied magnetic field in the y-axis direction and $H_0 = \Phi_0/\pi\lambda_{J_1}\Lambda_1$.

The system of nonlinear second order differential equations, Eq. (1), with the boundary conditions, Eq. (5), were solved numerically using a finite difference method.[9,16] The temperature dependence was introduced via temperature dependence of $J_{ci}(T)$ and $\lambda_{si}^{-2}(T)$, for which we have used a simple monotonous function $\sim 1-(T/T_c)^2$, typical for Nb.[18,19]

III. SAMPLES

The multilayered Nb/Cu sandwiches were fabricated on a single crystalline Si substrate. The sample consisted of thick top and bottom Nb electrodes, an isolating SiO_2 layer and the multilayer. The Nb/Cu ML's were prepared by rf sputtering. The ML's consist of ten Cu layers with the thickness $d_N = 15$ nm and ten Nb layers with the thickness $d_S = 20$ nm. Together with the superconducting electrodes this constitute ten stacked *SNS* (*S*: superconductor, *N*: normal metal) junctions. Sample layout and details of sample fabrication can be found in Ref. 20. The ML's were 20 μm in diameter. The transverse normal state resistance was several mΩ, which is larger than expected for uniform metallic film.[20] We attribute the enhanced values of resistance to the existence of additional tunnel resistances at the Nb/Cu interfaces which are inversely proportional to the interface transparency,[21] β. From calculation of the proximity effect in our ML's we estimate[19] $\beta \sim 0.3 \pm 0.1$. Therefore, the actual structure of our ML's is *SINIS* (*I*: insulator). In addition to the increase of transverse resistance, the finite β results in appearance of hysteresis[22] in the IVC's at low T, see inset in Fig. 5(a), and in large anisotropy,[23] $\gamma = 10-15$. Note, that the finite transparency was also reported for Nb/Al interfaces.[21] The existence of SJJ's in our ML's was confirmed by observation both ac (Ref. 20) and dc (Ref. 24) Josephson effects. We should note, that bulk *S* electrodes contribute to a screening of magnetic field and the actual field in the ML is less than the applied field. Magnetic[19,23] and transport[20,22,24,25] properties of our ML's both along and across layers have been studied and parameters of layers are rather well established. Both Nb and Cu layers are characterized by a short mean free path and are close to the dirty limit. From measurements of the lower[19,23] and the upper[24,23] critical fields, we can estimate the London penetration depth of Nb at $T = 0$ K to be $\lambda_{Nb}(0) \sim 120-150$ nm, and the Ginsburg-Landau parameter $\kappa \sim 10$. Thus, layers are much thinner than the London penetration depth and are of the order the coherence length.

The longitudinal transport measurements were carried out on a ML bridge with Cu as outmost layers to avoid surface superconductivity. The ML's then consisted of 12 Nb layers and 13 Cu layers.

For studying intrinsic Josephson effect in HTSC's, mesas with dimensions 20×10 and 50×10 μm^2 were fabricated on surfaces of Bi2212 single crystals. The mesas typically contain 4–10 intrinsic SJJ's. The patterning was made by photolithography and chemical etching. Several contacts on the top of the mesas allowed us to make four-probe measurements. More details about the sample fabrication and layout can be found elsewhere.[26] Bi2212 is a highly anisotropic layered superconductor. The anisotropy of transport properties in *ab* and *c* directions is very large, $\gamma \sim 10^3$, and depends on the doping level.[27] It is widely accepted, that in Bi2212, superconducting CuO double layers are weakly coupled through the intermediate SrO and BiO layers thus forming tunnel type intrinsic SJJ's.[27–29] Indeed, the *c*-axis IVC's exhibit a pronounced hysteresis with a well defined superconducting branch and multiple quasiparticle branches,[27–29] see inset in Fig. 5(b). Comparison of *c*-axis properties of Bi2212 with that of *SIS*-type LTSC Nb/AlO_x/Nb stacked Josephson junctions shows many similarities.[30,31] On the other hand, particular properties of intermediate layers may have a strong impact on the properties of intrinsic Josephson junctions. It is known that BiO layers act as a charge reservoir for the CuO layers. SrO layers most probably are inert. Certain experimental observations indicate that BiO layers may be metallic or even superconducting.[29] The properties of BiO layers strongly depend on the O-doping level. With increasing doping, the carrier concentration at BiO layers increases. This results in a decrease of anisotropy and the *c*-axis resistivity ρ_c, increase of the critical current I_c, and disappearance of hysteresis in the IVC's.[27,32] Similar or even more pronounced features were observed for Bi substituted compounds, such as $(Bi_{1-y}Pb_y)_2Sr_2CaCu_2O_{8+x}$, see Ref. 27. Therefore, Bi2212 can be considered as a stack of *SINIS* or $SI_1S_1I_2S_1I_1S$ junctions[29] (S_1 is a superconductor with lower T_c), rather than simply *SIS* junctions. Properties of *SNS* junctions depend strongly on properties of the normal layer and the transparency of the S/N interfaces. In Ref. 21, the general case of dirty $SI_1S_1IS_2I_2S$ single junction with arbitrary junction parameters was considered both theoretically and experimentally for Nb/Al_1/AlO_x/Al_2/Nb junctions. It was shown, that for the case of thin normal layers, $d_{S1,2} \leqslant \xi_{S1,2}$, with small interface transparency or low conductivity, the behavior of $SI_1S_1IS_2I_1S$ junction can be close to that of *SIS* junction. On the other hand, certain differences remain, e.g. a knee in the IVC just above the sumgap.[21,33] Therefore, it is interesting to make a comparison between Bi2212 and our Nb/Cu ML's, which as we mentioned above, have *SINIS* structure. Moreover, in our ML's the condition, $d \ll \lambda_S$, which is typical for HTSC, is satisfied much better than in typical artificial *SIS* SJJ's. Thus, SJJ's both in HTSC and in our ML's are in the strong electromagnetic coupling limit. Estimation of $\lambda_J(T=0)$ yields $\sim 0.5-1$ μm for Bi2212 and $\sim 4-5$ μm for Nb/Cu ML's, thus both HTSC and LTSC SJJ's are long compared to λ_J up to T very close to T_c.

IV. RESULTS AND DISCUSSION

Below we present transport measurements for different T and H. The samples were cooled in helium vapor and the temperature was stabilized by a temperature controller with an accuracy better than 0.05 K. For measurements below 4.2 K the sample was immersed into liquid He bath, connected

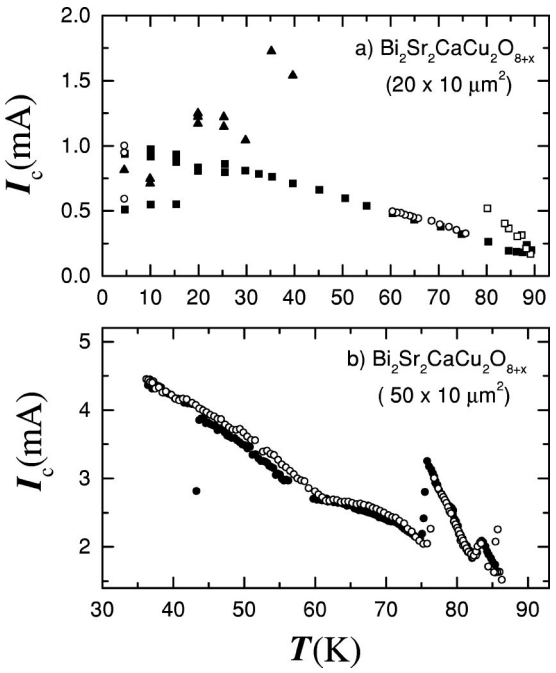

FIG. 1. Temperature dependence of the critical current for (a) 20 μm and (b) 50 μm long Bi2212 mesas. (a) represents results of statistical analysis with symbols corresponding to maxima in probability distribution. (b) represents single run measurements.

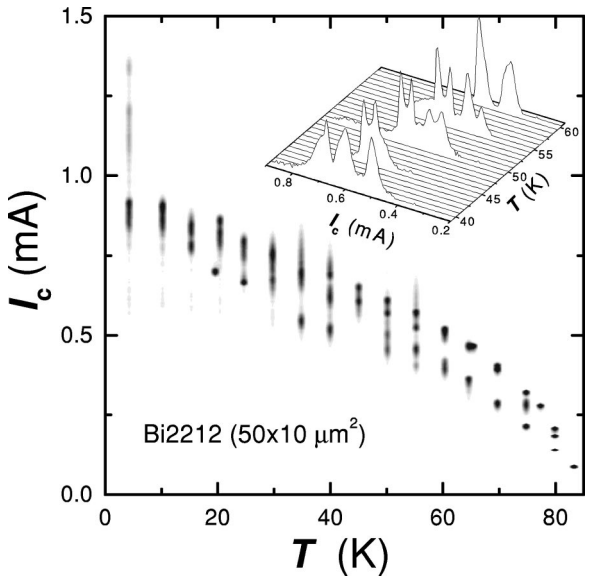

FIG. 2. A gray scale plot of the probability distribution $P(I_c)$ for a single temperature sweep for 50 μm long mesa. Darker regions correspond to a larger probability. Inset shows profiles $P(I_c)$ for several temperatures. Multiple peaks in $P(I_c)$ are seen.

to a monostat. The temperature was regulated from the pressure of He vapor. Magnetic field parallel to the layers was supplied by a superconducting solenoid, operating in a persistent mode for $H>1$ T. The accuracy of field alignment was about one degree. The noise level in the experimental setup was carefully checked to ensure that external noise is not a cause for observed anomalous behavior. To estimate the noise in the setup we measured the fluctuation induced escape temperature T_{esc} from the zero voltage state for a small LTSC Nb/NbO_x/Pb tunnel junction. At $T=4.2$ K, the estimated $T_{esc}\simeq 5$ K and the spread of the critical current was $\Delta I_c \sim 1.2\,\mu$A for a junction with $I_c \simeq 0.5$ mA.[17] This indicates a low external noise level in the setup.

A. Temperature dependence of the critical current

In Fig. 1, temperature dependence of the critical current is shown for Bi2212 mesas with lengths (a) 20 μm and (b) 50 μm. Measurements were done in an ambient magnetic field $\sim$0.5 Oe. Figure 1(b) represents ordinary measurement, in which I_c is obtained from a single switching event from the zero-voltage state. Normally we used a 1 μV criterion for determination of I_c. Solid and open symbols in Fig. 1(b) correspond to increasing and decreasing temperature, respectively.

As we mentioned, the statistical analysis of SJJ's is very important. Figure 1(a) shows $I_c(T)$ deduced from the probability distribution function $P(I_c)$. To obtain $P(I_c)$, 5120 switching events from the zero-voltage state were measured in a row[17] for each T. The I_c was determined as the maximum of $P(I_c)$. Typical switching events for a similar mesa at $T=4.2$ K and $H=0$ are indicated by arrows in inset in Fig. 5(b). Different symbols in Fig. 1(a) represent different temperature sweeps, all made while decreasing temperature from above T_c.

Figure 2 shows a gray scale plot of $P(I_c)$ for a single temperature sweep and for another 50 μm long mesa. Darker regions correspond to a larger probability. The inset in Fig. 2 shows profiles $P(I_c)$ for several temperatures in the range $40\,\mathrm{K}<T<60\,\mathrm{K}$.

From Figs. 1 and 2 it is seen that $I_c(T)$ for Bi2212 mesas is quite anomalous. For example, it is possible to observe a sudden decrease of I_c with decreasing T, see Fig. 1(b). The $I_c(T)$ is multiple valued and consists of several branches. The switching between branches is hysteretic. The $I_c(T)$ patterns depend on biasing configuration and show strong prehistory dependence, see Fig. 1(a). The characteristic feature of $I_c(T)$ patterns is extremely large fluctuations, which at certain T are of the order of the critical current itself. Such strong fluctuations can not be explained by external noise in the setup. Our estimation shows that for a single intrinsic Josephson junction with the same I_c as in Fig. 1(a), the external noise together with temperature induced fluctuations at $T=4.2$ K would correspond to a spread in I_c less than the size of symbols in Fig. 1(a). From Fig. 2 it is clearly seen that the probability distribution $P(I_c)$ is not simply wide, but it consists of several superimposed peaks, each peak representing a certain $I_c(T)$ branch.

The lower panel of Fig. 3 shows the perpendicular critical current, $I_c(T)$, for Nb/Cu ML. Different symbols correspond to different runs. Measurements were done at $H\sim 10$ mT along the layers. It is seen that I_c strongly fluctuates below $\sim$5 K. The top panel in Fig. 3 shows the upper critical field $H_{c2}(T)$ for H parallel (solid rectangles) and perpendicular (open circles) to the layers. H_{c2} was obtained from 50% of longitudinal resistive transition with the probe current applied along the layers.[24] The solid line in the top panel represents the square root dependence $(1-T/T^*)^{1/2}$. A linear-

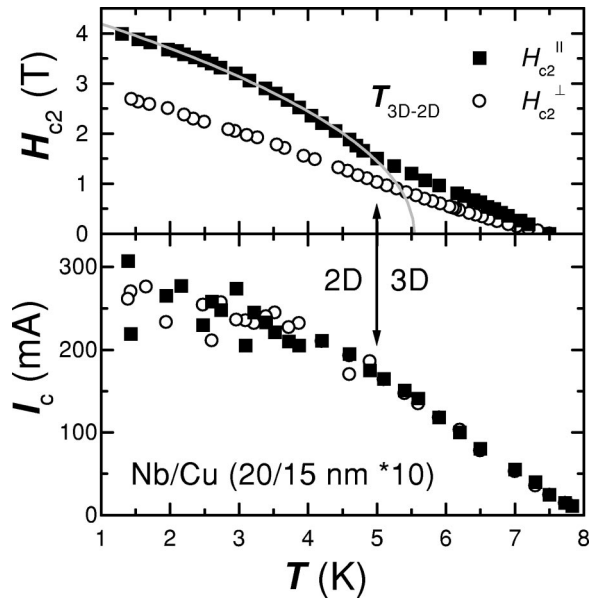

FIG. 3. The lower panel shows $I_c(T)$, for Nb/Cu multilayer. Different symbols correspond to different runs. The top panel shows the upper critical field $H_{c2}(T)$ for the field parallel (solid rectangles) and perpendicular (open circles) to the layers. The solid line represents a square root dependence, $(1-T/T^*)^{1/2}$. Arrows show that strong fluctuations of I_c take place below the crossover temperature.

to-square root transition in $H_{c2}^{\parallel}$ is seen, being the well known indication of the three-to-two (3D-2D) dimensional crossover.[34,35]

The 3D-2D crossover is one of the peculiar properties of superconducting ML's. The ML behaves as if being uniform across layers for $T>T_{cr}$ (3D state), while at lower temperatures (2D state) individual layers are distinguishable. The 3D-2D crossover was observed experimentally for various types of artificial LTSC multilayers, see, e.g., Ref. 34. Qualitatively, the 3D-2D crossover occurs[35] when the coherence length ξ_c, in the direction across layers becomes less than the interlayer spacing s. In our ML's, the 3D-2D crossover is well studied, see, e.g., Refs. 23, 20, 22, 24. It is important that in the 2D state, ''intrinsic'' Josephson effect between individual layers of the ML appears and the ML can be considered as a stack of Josephson junctions. Among the main observations of the Josephson phenomena in the 2D state in our Nb/Cu ML's we mention: (i) observation of Shapiro steps in the perpendicular IVC's showing the existence of ten SJJ's at low T.[20] (ii) Appearance of a hysteresis in the IVC's at low T (Refs. 22, 20) [see also inset in Fig. 5(a)] and a change in $I_c(T)$ behavior.[22] (iii) A steplike increase of the anisotropy of the lower critical field,[23] H_{c1}, at $T<T_{cr}$, caused by transformation of the vortex parallel to layers from Abricosov to Josephson type, when the vortex core could be imbedded between S layers. (iv) Appearance of the intrinsic pinning,[4] preventing vortex motion across the layers and resulting in a sharp drop of resistivity for H parallel to layers was observed in Ref. 24. (v) A clear periodic modulation of the transverse resistance as a function of parallel magnetic field was observed at $T\sim T_c$, with the periodicity given by flux quantization in the individual Nb/Cu/Nb junctions.[24] Finally, a direct observation of subdivision of our ML's into SJJ's with the 3D-2D crossover was made in Ref. 20.

The arrows in Fig. 3 show, that the appearance of strong fluctuations of I_c is connected with transition of the ML into the 2D state and appearance of SJJ's at $T<T_{cr}$. Similar to Bi2212, the existence of so large fluctuations cannot be explained neither by the noise in setup nor by temperature induced fluctuations in a single junction with the same I_c. Indeed, it is clear that the external noise does not depend on T, while temperature induced fluctuations should only decrease with decreasing T, in contrast to Fig. 3.

For Bi2212 we also observed a decrease of fluctuations at high temperature.[17] As a rule, we observed a very narrow peak in $P(I_c)$, close to T_c, see Fig. 2. An estimation shows that the 3D-2D crossover in Bi2212 should take place a few degrees below T_c. Indeed, $\sim$2 K below T_c the features of the intrinsic Josephson effect disappear, e.g., the quasiparticle branching and hysteresis in the IVC's vanish, similar to that for Nb/Cu ML's, see inset in Fig. 5(a) and flux-flow features in IVC's change the curvature.[36] Evidence for the 3D-2D crossover in Bi2212 and $YBa_2Cu_3O_{7-x}$ HTSC compounds were also obtained from magnetization measurements in Refs. 2, 37. The $P(I_c)$ pattern shown in Fig. 2 is consistent with the 3D-2D crossover taking place in Bi2212 close to T_c. On the other hand, for several mesas we observed, that the $P(I_c)$ may become narrow well below the estimated temperature of the 3D-2D crossover. This of course does not mean that the T_{cr} is lower for those mesas, but can be due to phase-locking of several junctions in the stack.[17]

To understand the observed features we have performed numerical simulations of the coupled sine-Gordon equation, Eq. (1), with boundary conditions given by Eq. (5). In Fig. 4 simulated $I_c(T)$ dependencies are shown for a stack of the overlap geometry,[8] consisting of three SJJ's for $H=0$. For simulations we have chosen parameters typical for our Bi2212 mesas $t_{1-3}=12$ Å, $d_{2-4}=3$ Å, $\lambda_J(T=0)=1\,\mu$m, the critical current densities J_{c1-3}, are identical and $L=10\,\mu$m. In order to account for the presence of a bulk single crystal beneath the mesa we take $d_1=10$ Å. The London penetration depth of S layers, $\lambda_{S1-4}(T=0)=750$ Å, was estimated from the expression[1,38] $\lambda_S=\lambda_{ab}\sqrt{d/s}$.

From Fig. 4 it is seen that $I_c(T)$ in long strongly coupled SJJ's is multiple valued and consist of multiple distinct branches, in qualitative agreement with the experiment, Fig. 1. Different symbols in Fig. 4 correspond to separate runs with increasing or decreasing temperature and/or different initial conditions. As seen from Fig. 4, we also observed hysteretic switching between branches and a prehistory dependence in our numerical simulations. Insets in Fig. 4 show the number of fluxons in junctions 1–3, $n_i=\Delta\varphi_i/2\pi$, where $\Delta\varphi_i=\varphi_i(L)-\varphi_i(0)$ is the total phase variation along the junctions. From the insets it is seen that each $I_c(T)$ branch corresponds to a particular phase distribution in the stack, i.e., to a particular fluxon mode. Four $I_c(T)$ branches corresponding to the Meissner state, mode (0,0,0), and three simplest fluxon-antifluxon modes, $(-1,1,0)$, $(0,-1,1)$, and $(1,0,-1)$, are marked in Fig. 4.

Previously, the existence of multiple valued I_c was shown for $H>H_{c1}$, when it is energetically favorable to have fluxons inside the stack.[17] The important difference of Fig. 4 is

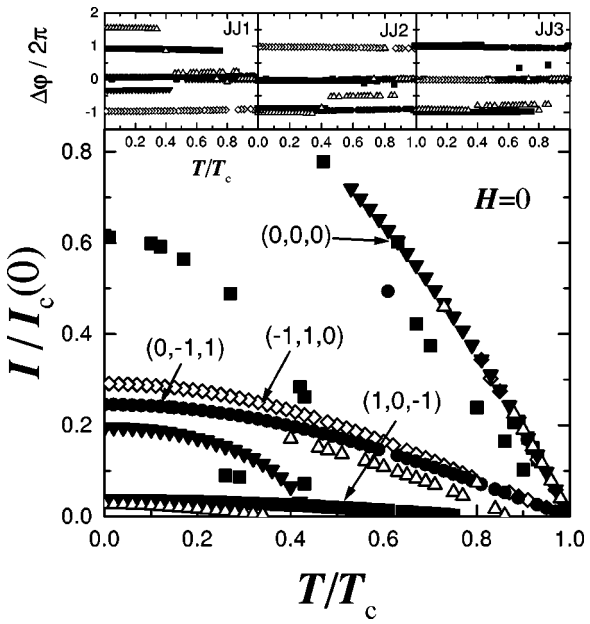

FIG. 4. Simulated $I_c(T)$ dependencies for three SJJ's with parameters typical for Bi2212 mesas and $H=0$. Different symbols correspond to separate runs with increasing or decreasing temperature and/or different initial conditions. Insets show the number of fluxons in the junctions. The $I_c(T)$ branches for (0, 0, 0) mode, and three simplest fluxon-antifluxon modes, $(-1, 1, 0)$, $(0, -1, 1)$, and $(1, 0, -1)$, are marked in the figure.

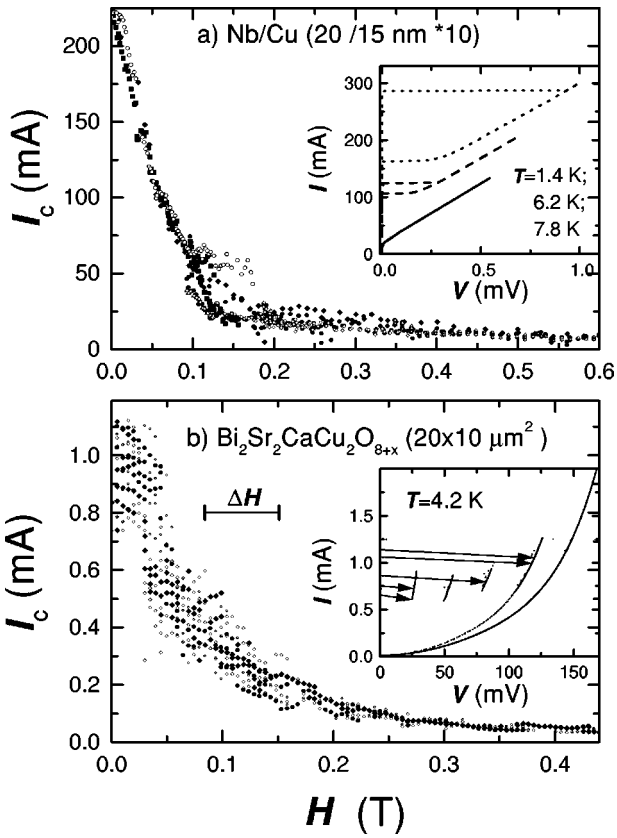

FIG. 5. The $I_c(H)$ dependencies at $T=4.2$ K are shown for (a) Nb/Cu ML and (b) Bi2212 mesa with $L=20\,\mu$m. In (a) different symbols represent different runs, each point representing a single measurement. (b) shows the result of statistical analysis with symbols representing maxima in $P(I_c)$. Inset in (a) shows IVC's of Nb/Cu ML at $T=1.4$, 6.2, and 7.8 K. Inset in (b) shows quasiparticle IVC's for Bi2212 mesa at $T=4.2$ K.

that here we considered fluxon-antifluxon modes and show that multiple branching of I_c sustain at $H=0$. Another difference is in the magnitude of I_c. In the presence of the unbound fluxon, there is a Lorentz force acting on the fluxon from the bias current and I_c is determined by the pinning at the edges of the junction. This results in a relatively small I_c. On the other hand, there is no net Lorentz force on the coupled fluxon-antifluxon pair and I_c is determined by the force required to unbound the pair. For example, the fluxon-antifluxon pair has a lower bound energy and a lower I_c for $(1,0,-1)$ than for $(-1,1,0)$ mode, see Fig. 4. The unbound force strongly depends on the electromagnetic coupling in the stack. As can be seen from Fig. 4, I_c can be a significant fraction of the maximum critical current, $I_c(0)$, for strongly coupled SJJ's.

For the real experimental situation, shown in Figs. 1–3, both fluxon and fluxon-antifluxon modes can be responsible for multiple valued I_c at $H=0$. For Bi2212 mesas we can expect a certain self-induced magnetic field due to nonuniform biasing, which is required for the four probe measurements. Indeed, we observed an asymmetry in IVC's for positive and negative currents, consistent with the self-field effect due to nonuniform bias.[39] For Nb/Cu ML's the self-field effect should be less pronounced, although we can not exclude it completely because of the large value of bias current.

B. Magnetic field dependence of the critical current

The dependence of the *c*-axis critical current on magnetic field in the *ab* plane $I_c(H)$, is a crucial test for the dc Josephson effect. In a single Josephson junction, Fraunhofer type modulation of $I_c(H)$ occurs as a result of flux quantization in the junction, with the periodicity

$$\Delta H=\Phi_0/L\Lambda^*, \tag{6}$$

where Λ^* is the effective magnetic thickness of the junction, Eq. (4). For SJJ's with thin layers $\Lambda^*\simeq s$. Similar periodic modulation should be observed for short SJJ's,[40,16] $L<\lambda_J$.

In Ref. 16, $I_c(H)$ for long strongly coupled SJJ's was considered. It was shown that the $I_c(H)$ pattern in this case is very complicated and does not exhibit clear periodicity due to existence of multiple quasiequilibrium fluxon modes and submodes.

Experimentally obtained $I_c(H)$ dependencies at $T=4.2$ K are shown in Fig. 5 for (a) Nb/Cu ML and (b) Bi2212 mesa with $L=20\,\mu$m. We note that for H parallel to the layers, a low resistance flux-flow branch developed in IVC's both for Nb/Cu ML's and Bi2212 mesas, see the next section. I_c was determined as a current, at which the first deviation from zero voltage appeared ($V\sim 1\,\mu$V), rather than the current at which switching from flux-flow to quasiparticle branch takes place. Inset in Fig. 5(a) shows IVC's of the Nb/Cu ML at $T=1.4$ K (dotted curve), 6.2 K (dashed curve), and 7.8 K (solid curve) at zero field. It is seen that pronounced hysteresis, with well defined superconducting and normal branches, exists at low temperatures. Another

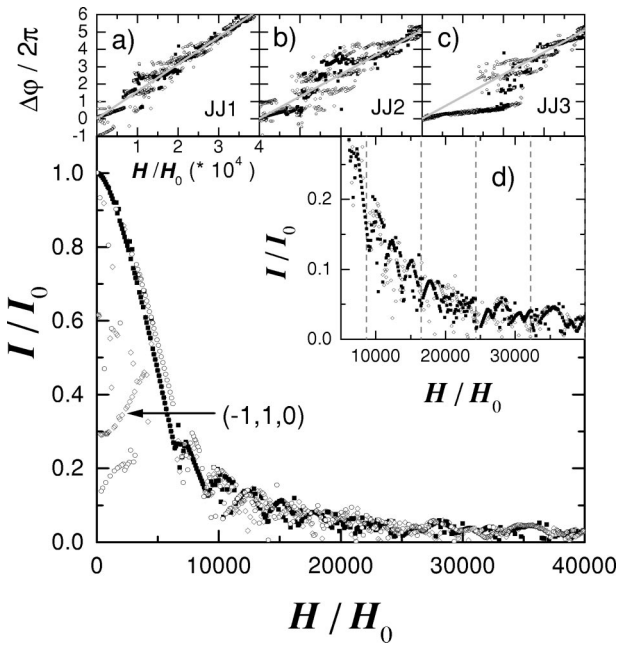

FIG. 6. Simulated $I_c(H)$ patterns for three SJJ's with parameters typical for Bi2212 mesas at $T=0$. Different symbols represent three different runs. Insets (a–c) show the number of fluxons in junctions 1–3, respectively. Solid lines represent the ''expected'' number of fluxons given by Eq. (5). Inset (d) shows details of $I_c(H)$ pattern at large H for two runs. Grid spacing is equal to ''expected'' periodicity, Eq. (6).

characteristic feature of IVC's is the excess current,[41,42] which indicates the proximity effect in our ML's, otherwise the IVC's are resembling that for resistively shunted junction (RSJ) model.[43] Inset in Fig. 5(b) shows quasiparticle branches for Bi2212 mesa at $T=4.2$ K. It is seen that the mesa consists of five intrinsic SJJ's. Arrows indicate some typical switching events from zero-voltage state for $H=0$.

In Fig. 5(a), different symbols represent different zero field cooled runs with increasing field. Each point represents a single measurement. Figure 5(b) shows the result of statistical analysis of I_c, similar to that in Fig. 1(a) and Fig. 2. In this case 2048 switching events from zero-voltage state were measured. I_c was determined[16] from the maximum of $P(I_c)$. Solid and open symbols in Fig. 5(b) represent main and secondary peaks in the probability distribution, circles and diamonds represent measurements with increasing and decreasing H, respectively. As in the case of Fig. 1(a) and Fig. 2, $P(I_c)$ was very wide and consisted of several maxima similar to that in inset of Fig. 2. From Fig. 5(b) it can be seen that fluctuations are reduced at large fields. At $H=0.45$ T the width of the probability distribution was about 2.5 μA, while at low fields it was almost 0.5 mA. Clearly the noise level in the setup does not decrease with increasing field and, thus, can not be the reason for the observed phenomenon.

Figure 6 presents the numerically simulated $I_c(H)$ pattern for the same stack as in Fig. 4 at $T=0$. Parameters are typical for our Bi2212 mesas. The magnetic field is normalized to $H_0=\Phi_0/\pi\lambda_{J2}\Lambda_2\sim 0.1-0.2$ Oe. Therefore, Figs. 5(b) and 6 have approximately the same scale in H. Different symbols in Fig. 6 represent three different runs, runs 1,2 for increasing (solid squares) and decreasing (open circles) field, starting from (0, 0, 0) mode. Run 3 (open diamonds) was made for increasing field starting from $(-1, 1, 0)$ mode. Insets (a)–(c) show the number of fluxons in junctions 1–3, respectively. Solid lines represent the ''expected'' number of fluxons given by Eq. (5). Inset (d) shows details of $I_c(H)$ pattern at large H for two runs from Fig. 6. Grid spacing in inset (d) is equal to the expected periodicity, ΔH, Eq. (6)

Several common features are seen in the behavior of $I_c(H)$ patterns for Nb/Cu ML, Bi2212 mesa, Fig. 5, and in numerical experiment, Fig. 6.

(i) I_c is strongly suppressed by the in-plane magnetic field. Fitting at large fields yields, $I_c \propto H^{-\eta}$, with $\eta=1.3\pm0.1$ for the Nb/Cu ML, $\eta=1.6\pm0.1$ for the Bi2212 mesa and $\eta=1.2\pm0.1$ for numerical simulations. The power law decrease of the maximum $I_c(H)$, with the exponent η, dependent on the sample geometry and bias conditions is typical for Josephson junctions.[44] The large suppression of I_c in Fig. 5 indicates that samples are properly oriented with respect to magnetic field, so that there are no pancake vortices in the *ab* planes which might cause the pinning of fluxons. For larger mesas the misorientation of the field was very crucial for $I_c(H)$ patterns. In that case, suppression of I_c was marginal, $I_c(H)$ remained almost constant or even increased with H as a result of pinning by pancake vortices. We note, that when the length of the mesa in the direction of the field is larger than some correlation length, pancake vortices can be nucleated by thermal fluctuations even if the sample is perfectly oriented.[3] Therefore, small area mesas are needed for the study of $I_c(H)$ patterns in HTSC intrinsic SJJ's.

(ii) From Figs. 5 and 6 it is seen, that I_c is multiple valued and $I_c(H)$ patterns consist of multiple closely spaced branches. Insets (a)–(c) in Fig. 6 show, that each branch is characterized by a certain fluxon distribution in the stack, i.e., corresponds to a certain fluxon mode or submode. The branch corresponding to $(-1, 1, 0)$ mode is marked in Fig. 6. In Fig. 6 we intentionally showed only three runs with a few sub-branches in order to identify the sub-branches with the corresponding fluxon modes in insets (a)–(c). More clearly, the sub-branches can be seen from inset (d) in Fig. 6, in which we showed only two runs with increasing field. In Ref. 16 it was shown, that the complete set of sub-branches is extremely dense even for the simplest case of double SJJ's.

(iii) The $I_c(H)$ patterns do not exhibit clear periodicity. For Nb/Cu ML at low T we observed strong history dependence in the variation of $I_c(H)$, but not the periodic modulation, see Fig. 5(a). Such behavior is consistent with the previous observation of aperiodic variation of the transverse resistivity, $R(H)$, see Ref. 24. However, in Ref. 24, a transition from aperiodic to periodic modulation of $I_c(H)$, with periodicity given by Eq. (6), was observed close to T_c for Nb/Cu ML's. Such transition was explained by disappearance of fluxon modes when the length of SJJ's becomes less than $\lambda_J(T)$. Indeed, numerical simulations show,[16] that the periodic modulation of $I_c(H)$ is restored when the stack becomes shorter than $\lambda_J(T)$, in agreement with Ref. 40. Similar modulation of $R(H)$ close to T_c was reported for $YBa_2Cu_3O_{7-x}$ in Ref. 45.

The statistical analysis of I_c for Bi2212 mesa in Fig. 5(b), provides us with more details and shows explicitly the existence of multiple I_c branches. However, looking at the overall shape of the $I_c(H)$ pattern, we may see only one clear

maximum at $H \sim 0.1$ T. Such behavior is consistent with previously obtained $I_c(H)$ patterns for Bi2212 mesas.[46] A mark in Fig. 5(b) shows the periodicity, ΔH, Eq. (6), expected for intrinsic Josephson junction. It would be very speculative to talk about such modulation both in experiment, Fig. 5(b), and in simulations, see inset (d) in Fig. 6.

In Ref. 16 it was shown, that the lack of periodicity in $I_c(H)$ pattern is caused by the existence of extremely large amount of fluxon modes and submodes. For example, the number of submodes for the stack of N junctions with M fluxons in total is[16]

$$m_s = N^M.$$

Comparison of the number of fluxons in the junctions with what expected for a given H, see solid lines in insets (a)–(c) of Fig. 6, shows, that neither the number of fluxons in each junction, nor the total number of fluxons in the stack are unambiguously determined by the value of applied magnetic field. Different fluxon modes and submodes have different critical currents. The $I_c(H)$ pattern is determined by the process of switching between different modes and submodes. In principle infinite number of modes and submodes makes the allowed values of I_c to be almost continuous leading to the lack of periodicity in $I_c(H)$. This does not mean that something is wrong with the dc Josephson effect in SJJ's but rather is a consequence of the electromagnetic coupling between the junctions.

C. The lower critical field and ineffectiveness of screening

An almost linear decrease of $I_c(H)$ at low fields in Fig. 6 corresponds to the Meissner state of the stack. At the end of the Meissner state fluxons enter one of the junctions in the stack. Normally, this happens at the lower critical field, H_{c1}. However, the Meissner state can hold up to $(\pi/2)H_{c1}$ due to the pinning at the edges of the junction.[44] The Meissner branch is splitted into sub-branches, with each sub-branch corresponding to the entrance of a single fluxon into one of the junctions. We can attribute a particular H_{c1i} to each junction as a field at which the mode $(0,...,n_i=1,...,0)$ becomes energetically favorable,[8] and define the lower critical field as $H_{c1} = \min(H_{c1i})$. A small splitting corresponding to (1, 0, 0) and (0, 1, 0) modes is seen in Fig. 6. In this case, splitting is caused by the difference in effective magnetic thicknesses, Λ_i^*, Eq. (4). This leads to the difference in the total flux carried by the fluxon, and consequently to the difference in H_{c1i}, see Ref. 8. A more dramatic splitting of the Meissner state can be obtained[16] for junctions with different J_{ci}.

We would like to note that the splitting of the Meissner branch in strongly coupled SJJ's (i.e., with thin S layers) remains even if parameters of the junctions are identical (the only exception is identical double SJJ's). The reason is that for $d \ll \lambda_{ab}$, the magnetic field of the fluxon is not confined in one junction, but is spread over the region $\sim\lambda_{ab}$ in the c axis.[5,6] This makes junctions different with respect to position in the c-axis direction. Indeed, for a stack with $N \gg 1$, the total flux of the fluxon in the middle junction is Φ_0, while it is only $\Phi_0/2$ for the utmost junctions. Since H_{c1i} is inversely proportional to the total flux carried by the fluxon,[8] this result in a factor of 2 difference in H_{c1i} and splitting of the Meissner branch.

For Nb/Cu ML's, an almost linear Meissner branch with a small splitting is seen in Fig. 5(a). From Fig. 5(b) it is seen that for Bi2212 mesa there is a drop in $I_c(H)$ at $H \sim 0.05$ T. Comparison of $I_c(H)$ for mesas with different lengths shows that the position of this drop does not change with L. Therefore, we suggest that this drop represents H_{c1}. Indeed, a droplike decrease of $I_c(H)$ is typical for junctions with self-field effect due to nonuniform biasing,[39] which is the case for our mesas.

From Fig. 6 it is seen that multiple sub-branches $I_c(H)$ exist also inside the Meissner region, $H < H_{c1}$. Those sub-branches correspond to various fluxon and especially fluxon-antifluxon modes and submodes, see Fig. 4. Sub-branching at $H < H_{c1}$ is also observed for Bi2212 mesas, see Figs. 1 and 5(b). As we discussed in the previous section, fluxon-antifluxon modes and submodes are the likely candidates for explaining this phenomenon. However, splitting of the Meissner branch and fluxon modes due to self-field effect cannot be excluded.

Another interesting observation from Fig. 6 is that $H_{c1} \gg H_0 \sim 0.1-0.2$ Oe. We note, that for a single junction with bulk electrodes $H_{c1} = (2/\pi)H_0$, see Ref. 44. However, as d becomes less than λ_s, H_{c1} increases proportional to $\Lambda/\Lambda^* \sim \lambda_s^2/(ds)$ for $d \ll \lambda_s$, although the magnetic induction in the center of the fluxon remains $\sim H_0$, see Ref. 8. The dramatic increase of H_{c1} is an indication of ineffectiveness of screening in junctions with thin S layers. Magnetic field penetrates such junctions almost freely without generation of large phase difference.

The ineffectiveness of screening in our Bi2212 mesas containing only five intrinsic SJJ's, can be seen from Fig. 5(b). Indeed, the value $H_{c1} \sim 0.05$ T is about two orders of magnitude larger than H_{c1} for bulk Bi2212 single crystals.[12] For Nb/Cu ML we also observed a large value of H_{c1}, however, the effect is larger than we can expect, probably due to screening from bulk Nb electrodes.

D. Multiple flux-flow sub-branches

So far we have considered only the static case. In this section we analyze the dynamic behavior of our samples. In the dynamic case, the c-axis transport current forces fluxon motion along the layers which causes appearance of the c-axis voltage. Time averaged voltage across the junction is proportional to the velocity and the number of fluxons in the junction. For large H, the ratio V/H for fluxon motion with velocity u in the stack of N junctions can be estimated as

$$V/H = Nsu. \tag{7}$$

For single Josephson junction, the maximum velocity of fluxon is equal to the Swihart velocity c_0, which is the velocity of electromagnetic waves in the transmission line formed by the junction. Fluxon velocity asymptotically approaches c_0 with increasing I, resulting in appearance of an almost vertical step in IVC at the velocity matching condi-

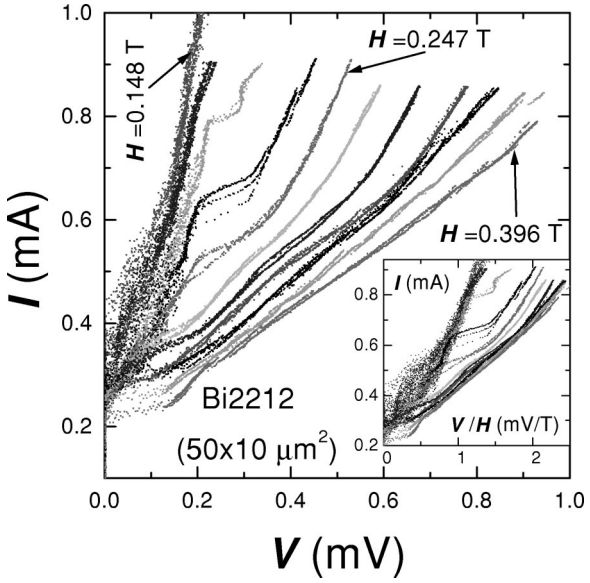

FIG. 7. Flux-flow IVC's of 50 μm long Bi2212 mesa at $T=4.2$ K are shown for H from 0.148 to 0.396 T with a step $\simeq 0.025$ T. In inset, I vs V/H curves are plotted for the same IVC's.

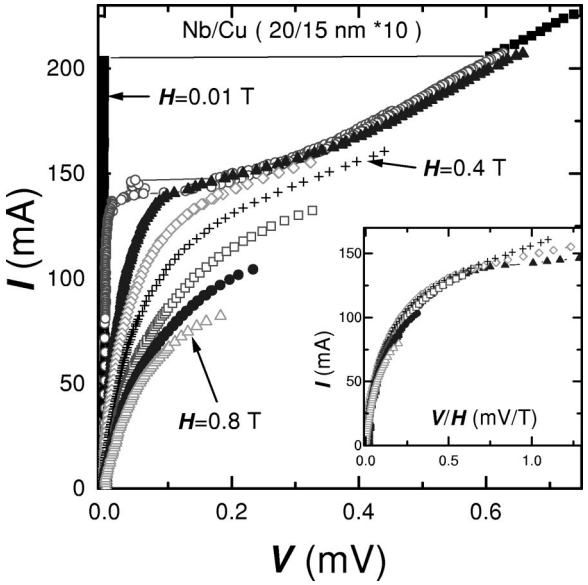

FIG. 8. IVC's of Nb/Cu multilayer at $T=4.2$ K are shown for different magnetic fields. In inset, I vs V/H curves are plotted for the same IVC's.

tion, $u \rightarrow c_0$, see, e.g., Ref. 47. The characteristic feature of SJJ's is the splitting of Swihart velocities and flux-flow IVC's.[7,48,49]

In Fig. 7, IVC's of the 50 μm long Bi2212 mesa are shown for H from 0.148 to 0.396 T with a step $\simeq 0.025$ T, at $T=4.2$ K. Magnetic field was applied along the *ab* plane and perpendicular to the longest side of the mesa. The IVC for each H contains about a hundred back and forth sweeps. From Fig. 7 it is seen, that a low resistance branch develops in the IVC's and the voltage at a constant I is increasing with H. Moreover, V/H does not depend on the length of the mesa. This is in agreement with Eq. (7). Therefore, we identify those low resistance branches with Josephson flux-flow branches (JFFB's). The same IVC's, normalized to H are shown in the inset. We note, that for a single junction the V/H vs I curves should collapse into one. For our mesa we observe instead, that there are two distinct IFFB's with approximately a factor of 2 difference in the voltages.[50] At low fields the curves collapse into the lower branches. At $H=0.223$ T the IVC follows the initial lower branch up to $I \simeq 0.6$ mA. However, when increasing the current further, the IVC jumps to the second branch with higher resistance. The switching is hysteretic. At larger fields the normalized IVC's collapse to the upper branch. The existence of two JFFB's may be an indication for the phase transition in fluxon configuration and/or the splitting of Swihart velocities in intrinsic SJJ's.[50] The 20 μm long mesa on the same single crystal showed the same values of V/H, although IVC's were more complicated due to the presence of Fiske steps.[51]

In Fig. 8, IVC's of Nb/Cu ML are shown for $H=0.01$, 0.05, 0.13, 0.26, 0.4, 0.56, 0.7, and 0.8 T, at $T=4.2$ K. Each curve represents a single current sweep. In inset we show I vs V/H curves for the same IVC's. It is seen that I vs V/H curves merge well into a single curve. On the other hand, the curvature of I vs V/H curves is negative for Nb/Cu ML and positive for HTSC mesas. The negative curvature for Nb/Cu ML's can be explained within the RSJ model[43] by the large damping coefficient in these *SNS* junctions.

From Fig. 7 it is seen that the JFFB's are rather wide. At small voltages, the spread in IVC's reflects fluctuations in I_c, as discussed in Sec. IV A. At larger voltages, the spread in IVC's somewhat decreases, but still remains anomalously large.

In Fig. 9 we show an enlarged top part of I vs $R=V/I$ curves of the 50 μm long Bi2212 mesa for magnetic fields varying in small steps of $\simeq 5$ mT in the range $H=0.351-0.396$ T, at $T=4.2$ K. The I vs R curve for each H is shown by a particular color and contains several tens back and forth current sweeps. From Fig. 9 it is seen, that I vs R curves and, similarly, IVC's for a fixed H exhibit strong

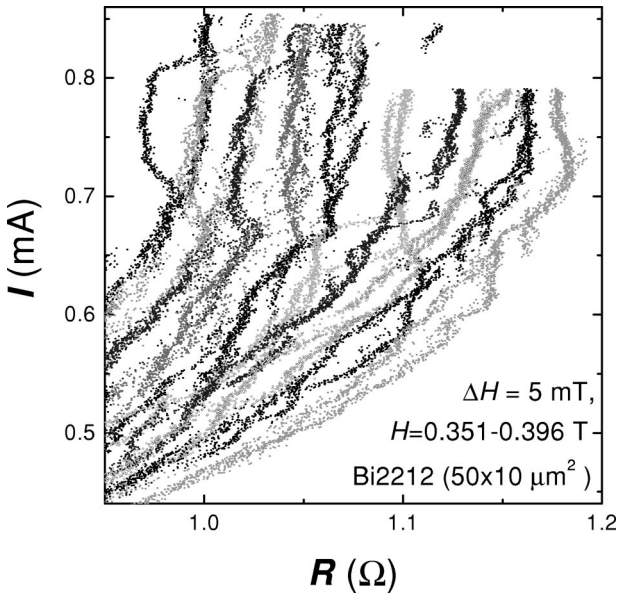

FIG. 9. Enlarged top parts of I vs $R=V/I$ curves of 50 μm long Bi2212 mesa are shown for H varying with a small step $\simeq 5$ mT in the range $H=0.351-0.396$ T, at $T=4.2$ K. The curve for each H is shown by a particular color.

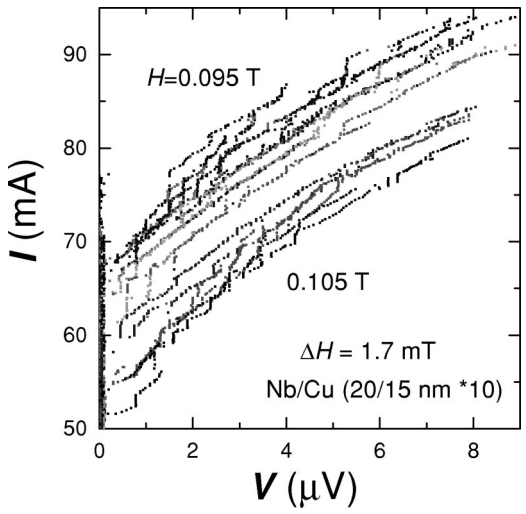

FIG. 10. Enlarged parts of IVC's for Nb/Cu multilayer at $T=4.2$ K are shown for $H=0.095-0.105$ T, varying with a small step $\simeq 1.7$ mT.

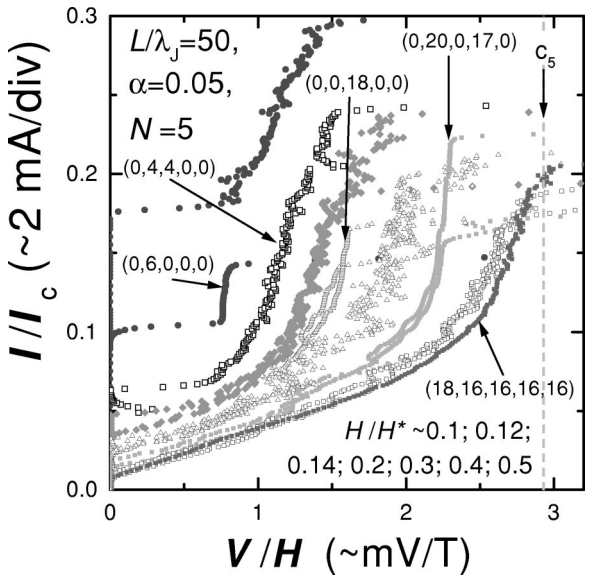

FIG. 11. Numerically simulated I vs V/H curves for Bi2212 mesas at several H. Typical fluxon modes along the flux-flow branches are depicted.

fluctuations. The spread in voltages is not caused by the noise in experimental setup and exceeds by far the accuracy of the measurements. The characteristic feature of I vs R curves from Fig. 9 and IVC's from Fig. 7 is that the curves are not just uniformly wide, but rather they consist of multiple closely spaced but distinct sub-branches. The IVC's switch hysteretically between the sub-branches when the current is swept back and forth. Varying H, we only change the set of available sub-branches but do not change the shape of the particular sub-branch itself. Another characteristic feature of Fig. 9 is that certain sub-branches exhibit steps of almost constant resistance.

In Fig. 10 we show IVC's of Nb/Cu ML for magnetic fields varying with a small step $\simeq 1.7$ mT in the range $H=0.095-0.105$ T, at $T=4.2$ K. The IVC's for each H contain several current sweeps. As in the case of HTSC, Fig. 9, we also observe that flux-flow branches in IVC's consist of multiple closely spaced but distinct sub-branches. Steps with almost constant voltage in Fig. 10 may represent geometrical resonances.

Previously, similar multiple flux-flow sub-branches were observed for LTSC Nb/Cu multilayers[24] and HTSC mesas.[52] Multiple jumps in transverse resistance as a function of H related to switching between different sub-branches were also observed for Nb/Cu ML's (Ref. 24) and $YBa_2Cu_3O_{7-x}$.[45] The known reason for the existence of multiple branches in IVC's of Josephson junctions is geometrical resonances. In IVC's of long junctions, geometric resonances are represented by a dense set of Fiske steps with constant voltage, see, e.g., Ref. 53, and references therein. For long SJJ's, voltage spacing between various Fiske steps may decrease with respect to a single junction due to the splitting of Swihart velocities and appearance of two-dimensional geometric resonances.[48] The splitting was observed for LTSC SJJ's (Refs. 49, 30) and could be responsible for the dense step structure in Fig. 10. For Bi2212 mesas, the Fiske step structure in IVC's was observed in Ref. 51 However, geometrical resonances can hardly explain multiple sub-branches, shown in Figs. 9 and 10. Indeed, the sub-branches in Fig. 9 do not show steps of constant voltage, but have rather large and almost constant resistance. Figure 10 shows that step structure and multiple flux-flow sub-branches may coexist but do not reduce to each other.

In Ref. 52 it was suggested that sub-branching is due to splitting of Swihart velocities and propagation of different phases of the fluxon lattice. Indeed, the splitting of Swihart velocities can cause the splitting of JFFB's, so that for the stack of N junctions, N universal JFFB's may be visible in I vs V/H curves, each corresponding to propagation of different phases of FL's with different Swihart velocities. The splitting of Swihart velocities decreases as N^{-2} at the low velocity edge, and for SJJ's with $N \gg 1$ may result in appearance of a dense system of JFFB's.

However, measurements on mesas with a large number of SJJ's ($N=250$ for the case of Ref. 52) do not allow to make a decisive conclusion about the origin of the multiple flux-flow sub-branches. In our mesas with the small number of SJJ's, $N=5$, splitting of Swihart velocities becomes large. This splitting is almost two orders of magnitude larger than the splitting visible in Fig. 9. We should also note that the number of sub-branches is not limited by the number of SJJ's in the mesa. All this rules out the explanation of multiple flux-flow sub-branches observed here, in terms of the splitting of Swihart velocities.

In Ref. 24 it was proposed that multiple flux-flow sub-branches represent propagation of different fluxon modes. The number of fluxons and the propagation velocities of different modes are basically different. Therefore, closely spaced flux-flow sub-branches, with the total number (much) larger than the number of junctions in the stack[8] may appear. Recently the existence of multiple fluxon modes in the dynamic state of SJJ's was supported by direct numerical simulations.[54]

Figure 11 represents numerical modeling of the I vs V/H curves for our Bi2212 mesas. In the simulations we have chosen parameters typical for our mesas: $N=5$, $J_c \sim 10^3$ Å/cm^2, $s=15$ Å, $d=3$ Å, and $\lambda_J \sim 0.5-1$ μm. The parameters of JJ's were identical, except for larger thickness

of the bottom electrode, $d_1 = 6$ Å, in order to imitate the bulk crystal beneath the mesa. The damping parameter was $\alpha = 0.05$. V and H are normalized to $V_0 = (\Phi_0/2\pi c)c_0/\lambda_J \sim 0.2$ mV and $H_0 = \Phi_0/\pi\Lambda\lambda_J \sim 0.2$ Oe, respectively. Figure 11 reproduces quantitatively the experimental V/H values, see Fig. 7. At large H the curves merge into one. Here the top fluxon velocity is close to the lowest Swihart velocity,[48,30] c_5, as indicated by the dashed vertical line. At small H the flux-flow voltage is strongly fluctuating and tiny sub-branches can be found after closer examination. Those sub-branches correspond to propagation of different quasiequilibrium fluxon modes,[8,24] characterized by different fluxon distributions in the stack. Typical modes are indicated in Fig. 11 for selected IVC's. Both the number of fluxons and propagation velocities of different modes are in general different. Certain probability for realization of different fluxon modes results in fluctuations of flux-flow voltage and appearance of multiple flux-flow sub-branches. The fluxon lattice becomes stable only at large fields, see mode (18, 16, 16, 16, 16) at $H \sim 0.5$ T in Fig. 11. More detailed analysis of JFFB's in SJJ's can be found in Ref. 54. Switching between the fluxon modes and submodes and correlated fluctuations of the flux-flow voltage due to switching between flux-flow sub-branches is a likely alternative reason for the broadband radiation from intrinsic SJJ's.[55]

V. CONCLUSIONS

In conclusion, the *c*-axis static and dynamic properties of HTSC $Bi_2Sr_2CaCu_2O_{8+x}$ mesas and LTSC Nb/Cu multilayers were studied experimentally and numerically. We found that both HTSC mesas and LTSC multilayers exhibit similar anomalous properties: (i) The *c*-axis critical current is multiple valued as a function of temperature, Figs. 1–3, and in-plane magnetic field, Fig. 5, and consists of multiple sub-branches $I_c(T,H)$. (ii) The critical current exhibits extremely large fluctuations and probability distribution $P(I_c)$ has multiple maxima, Fig. 2. (iii) The $I_c(H)$ patterns are aperiodic, Fig. 5. (iv) In the dynamic state, the flux-flow IVC's consist of multiple closely spaced sub-branches and exhibit large fluctuations due to switching between the sub-branches. Experimental data are in good agreement with numerical simulations for the stack of long strongly coupled Josephson junctions. All this is taken as experimental evidence for the existence of multiple quasiequilibirium fluxon modes in intrinsic SJJ's both in static and dynamic states. Fluxon modes/submodes represent different quasiequilibrium fluxon configurations.[8,16] Due to the existence of multiple fluxon modes and submodes the state of the stack is not well defined, but can only be described statistically with a certain probability of being in any of the quasiequilibrium states. Therefore, we emphasize the importance of statistical analysis of experimental data for long strongly coupled SJJ's. Measurements of model LTSC multilayers allow us to unambiguously relate the anomalous behavior with appearance of ''intrinsic'' SJJ's in the 2D state.

ACKNOWLEDGMENTS

The work was supported by NWO Grant No. 047.005.001.97, INTAS Grant No. 96-0452, and BMBF Grant No. 13N6943/3.

*Present address: Department of Microelectronics and Nanoscience, Chalmers University of Technology, S-41296 Göteborg, Sweden.

†On leave from P. L. Kapitza Institute, Kosygina 2, 117334 Moscow, Russia.

‡Also at IMEGO Institute, Aschebergsgatan 46, S-41133 Göteborg, Sweden.

[1] J. Clem, Phys. Rev. B **43**, 8737 (1991).
[2] G. Blatter, M. V. Feigelman, V. B. Geshkenbein, A. I. Larkin, and V. M. Vinokur, Rev. Mod. Phys. **66**, 1125 (1994).
[3] L. Balents and D. R. Nelson, Phys. Rev. B **52**, 12 951 (1995).
[4] M. Tachiki and S. Takahashi, Solid State Commun. **70**, 291 (1989).
[5] J. Clem and M. Coffey, Phys. Rev. B **42**, 6209 (1990).
[6] V. M. Krasnov, N. F. Pedersen, and A. A. Golubov, Physica C **209**, 579 (1993).
[7] S. Sakai, P. Bodin, and N. F. Pedersen, J. Appl. Phys. **73**, 2411 (1993).
[8] V. M. Krasnov and D. Winkler, Phys. Rev. B **56**, 9106 (1997).
[9] V. M. Krasnov, Phys. Rev. B **60**, 9313 (1999); V. M. Krasnov and D. Winkler, *ibid.* **60**, 13 179 (1999).
[10] L. S. Levitov, Phys. Rev. Lett. **66**, 224 (1991).
[11] V. M. Krasnov, V. A. Larkin, and V. V. Ryazanov, Physica C **174**, 440 (1991).
[12] N. Nakamura, G. D. Gu, and N. Koshizuka, Phys. Rev. Lett. **71**, 915 (1993).
[13] G. I. Watson and G. S. Canright, Phys. Rev. B **48**, 15 950 (1993).
[14] S. E. Shafranjuk, M. Tachiki, and T. Yamashita Phys. Rev. B **57**, 13 765 (1998).
[15] X. Hu and M. Tachiki, Phys. Rev. Lett. **80**, 4044 (1998).
[16] V. M. Krasnov, N. Mros, A. Yurgens, and D. Winkler, Physica C **304**, 172 (1998).
[17] N. Mros, V. M. Krasnov, A. Yurgens, D. Winkler, and T. Claeson, Phys. Rev. B **57**, R8135 (1998).
[18] D. K. Finnemore, T. F. Stromberg, and C. A. Swenson, Phys. Rev. Lett. **149**, 231 (1966).
[19] V. M. Krasnov, V. A. Oboznov, and V. V. Ryazanov, Physica C **196**, 335 (1992).
[20] V. M. Krasnov, N. F. Pedersen, V. A. Oboznov, and V. V. Ryazanov, Phys. Rev. B **49**, 12 969 (1994).
[21] A. A. Golubov, E. P. Houwman, J. G. Gijsbertsen, V. M. Krasnov, J. Flokstra, and H. Rogalla, Phys. Rev. B **51**, 1073 (1995).
[22] V. M. Krasnov, N. F. Pedersen, and V. A. Oboznov, Phys. Rev. B **50**, 1106 (1994).
[23] V. M. Krasnov, A. E. Kovalev, V. A. Oboznov, and V. V. Ryazanov, Physica C **215**, 265 (1993).
[24] V. M. Krasnov, A. E. Kovalev, V. A. Oboznov, and N. F. Pedersen, Phys. Rev. B **54**, 15 448 (1996).
[25] P. Seng, R. Tidecks, K. Samwer, G. Yu. Logvenov, and V. A. Oboznov, J. Low Temp. Phys. **106**, 29 (1997).
[26] A. Yurgens, D. Winkler, T. Claeson, and N. V. Zavaritsky, Appl. Phys. Lett. **70**, 1760 (1997).
[27] R. Kleiner and P. Mueller, Phys. Rev. B **49**, 1327 (1994).
[28] R. Kleiner, F. Steinmeyer, G. Kunkel, and P. Mueller, Phys. Rev. Lett. **68**, 2394 (1992).
[29] A. Yurgens, D. Winkler, N. V. Zavaritsky, and T. Claeson, Phys. Rev. B **53**, R8887 (1996).

[30] S. Sakai, A. V. Ustinov, H. Kohlstedt, A. Petraglia, and N. F. Pedersen, Phys. Rev. B **50**, 12 905 (1994).
[31] R. Kleiner, P. Müller, H. Kohlstedt, N. F. Pedersen, and S. Sakai, Phys. Rev. B **50**, 3942 (1994).
[32] K. Schlenga, R. Kleiner, G. Hechtfischer, M. Mößle, S. Schmitt, P. Müller, Ch. Helm, Ch. Preis, F. Forsthofer, T. Keller, H. L. Johnson, M. Veith, and E. Steinbeiß, Phys. Rev. B **57**, 14 518 (1998).
[33] A. A. Golubov and M. Yu. Kupriyanov, J. Low Temp. Phys. **70**, 83 (1988).
[34] I. Banerjee and I. K. Schuller, J. Low Temp. Phys. **54**, 501 (1984).
[35] S. Takahashi and M. Tachiki, Phys. Rev. B **33**, 4620 (1986).
[36] J. U. Lee and J. E. Nordman, Physica C **277**, 7 (1997).
[37] N. E. Hussey, J. R. Cooper, C. Changkang, and J. W. Hodby, Physica C **292**, 218 (1997).
[38] A. A. Golubov and V. M. Krasnov, Physica C **196**, 177 (1992).
[39] V. M. Krasnov, V. A. Oboznov, and N. F. Pedersen, Phys. Rev. B **55**, 14 486 (1997).
[40] L. N. Bulaevskii, J. R. Clem, and L. I. Glazman, Phys. Rev. B **46**, 350 (1992).
[41] G. E. Blonder, M. Tinkham, and T. M. Klapwijk, Phys. Rev. B **25**, 4515 (1982).
[42] A. A. Golubov, V. M. Krasnov, and M. Yu. Kupriyanov, J. Low Temp. Phys. **106**, 249 (1997).
[43] K. K. Likharev, *Dynamics of Josephson Junctions and Circuits* (Gordon and Breach, New York, 1986).
[44] A. Barone and G. Paterno, *Physics and Applications of the Josephson Effect* (Wiley, New York, 1982).
[45] D. C. Ling, G. Yong, J. T. Chen, and L. E. Wenger, Phys. Rev. B **75**, 2011 (1995).
[46] Yu. I. Latyshev, J. E. Nevelskaya, and P. Monceau, Phys. Rev. Lett. **77**, 932 (1996).
[47] D. W. McLaughlin and A. C. Scott, Phys. Rev. A **18**, 1652 (1978).
[48] R. Kleiner, Phys. Rev. B **50**, 6919 (1994).
[49] A. V. Ustinov, H. Kohlstedt, M. Cirillo, N. F. Pedersen, G. Hallmanns, and C. Heiden, Phys. Rev. B **48**, 10 614 (1993).
[50] V. M. Krasnov, N. Mros, A. Yurgens, and D. Winkler, IEEE Trans. Appl. Supercond. **9**(2), 4499 (1999).
[51] V. M. Krasnov, N. Mros, A. Yurgens, and D. Winkler, Phys. Rev. B **59**, 8463 (1999).
[52] J. U. Lee, P. Guptasarma, D. Hornbaker, A. El-Kortas, and K. E. Gray, Appl. Phys. Lett. **71**, 1412 (1997).
[53] M. Cirillo, N. Grønbech-Jensen, M. R. Samuelsen, M. Salerno, and G. Verona Rinati, Phys. Rev. B **58**, 12 377 (1998); V. P. Koshelets, S. V. Shitov, A. V. Shchukin, L. V. Filippenko, J. Mygind, and A. V. Ustinov, *ibid.* **56**, 5572 (1997).
[54] V. M. Krasnov, N. Mros, A. Yurgens, and D. Winkler, Physica B (to be published).
[55] G. Hechtfisher, R. Kleiner, A. V. Ustinov, and P. Mueller, Phys. Rev. Lett. **79**, 1365 (1997).